



저작자표시-비영리-변경금지 2.0 대한민국

이용자는 아래의 조건을 따르는 경우에 한하여 자유롭게

- 이 저작물을 복제, 배포, 전송, 전시, 공연 및 방송할 수 있습니다.

다음과 같은 조건을 따라야 합니다:



저작자표시. 귀하는 원저작자를 표시하여야 합니다.



비영리. 귀하는 이 저작물을 영리 목적으로 이용할 수 없습니다.



변경금지. 귀하는 이 저작물을 개작, 변형 또는 가공할 수 없습니다.

- 귀하는, 이 저작물의 재이용이나 배포의 경우, 이 저작물에 적용된 이용허락조건을 명확하게 나타내어야 합니다.
- 저작권자로부터 별도의 허가를 받으면 이러한 조건들은 적용되지 않습니다.

저작권법에 따른 이용자의 권리는 위의 내용에 의하여 영향을 받지 않습니다.

이것은 [이용허락규약\(Legal Code\)](#)을 이해하기 쉽게 요약한 것입니다.

[Disclaimer](#)

Thesis for the Degree

Master of Education

Surface phenomena of ZrO_2 coated Si

**(100) at different substrate
temperatures**



by

Misun Chun

Graduate School of Education

Pukyong National University

August 2009

**Surface phenomena of ZrO_2 coated Si
(100) at different substrate
temperatures**

실리콘에 코팅된 ZrO_2 의 온도에
따른 표면현상에 관한 연구

Advisor : Prof. Yong-Cheol Kang

by

Misun Chun

A thesis submitted in partial fulfillment of the requirements
for the degree of

Master of Education

Graduate School of Education
Pukyong National University

August 2009

**Surface phenomena of ZrO_2 coated Si (100) at different
substrate temperatures**

A dissertation

by
Misun Chun

Approved by :

Chairman : Ju Chang Kim

Member : Sang Yong Pyun

Member : Yong-Cheol Kang

August 26, 2009

Contents

List of Figures	iii
List of Tables	vi
Abstract	vii
I . Introduction	1
II . Theory	3
2.1 X-ray photoelectron spectroscopy (XPS)	3
2.1.1 Vacuum system	4
2.1.2 X-ray sources	4
2.1.3 XPS principle	5
2.1.4 Photoemission process	6
III. Experimental	8
3.1 Experimental apparatus and procedure	8
3.2 Instrumental analysis of Zirconium oxide thin films ...	10
3.2.1 The experimental condition of XPS	10
3.2.2 Deconvolution of Zr 3d and O 1s	11

3.2.3 The experimental condition of XRD	11
3.2.4 The experimental condition of AFM and SE	12
IV. Results and Discussion	13
4.1 XPS of Zirconium oxide	13
4.2 XRD of Zirconium oxide	27
4.3 AFM of Zirconium oxide	29
4.4 SE of Zirconium oxide	31
V. Conclusion	32
VI. Reference	33
Korean Abstract	37
Acknowledgment	38

List of Figures

Figure 2.1.1	Schematic diagram of the XPS process, showing photoionization of an atom by the ejection of a 1s electron.	6
Figure 3.1.1	Schematic representation of RF magnetron sputtering chamber.	9
Figure 4.1.1	The survey XPS of zirconium oxide on Si (100) before and after zirconium oxide deposition and substrate annealing.	14
Figure 4.1.2	(a) stacked XP spectra of the Zr 3d _{5/2} and 3d _{3/2} which zirconium oxide thin film on Si (100) with increased substrate temperature.	17
	Deconvoluted XP spectra of the Zr 3d when silicon substrate temperature at 623K (b) and 293K (c). The Zr 3d spectrum was separated three oxidation state; zirconium oxide (ZrO ₂), higher oxidation state and lower oxidation state. The spots represent raw data, smooth lines mean sum of deconvoluted Zr 3d.	18

Figure 4.1.3 (a) XP spectra of the O 1s region zirconium oxide on Si 21

(100) with different substrate heating temperature. The silicon dioxide (SiO₂) peak was assigned at 531.7 eV, and the zirconium oxide (Zr-O) was assigned at 529.6 eV.

Deconvoluted XP spectra of the O 1s when silicon 22

substrate temperature was 623K (b) and 293K (c). The O 1s spectra were separated four oxidation state; zirconia (ZrO₂), higher and lower oxidation state (ZrO_x), surface oxygen (-OH), silicon oxide (SiO₂). The bottom solid lines are background.

Figure 4.1.4 The relative ratios of the Zr 3d (a) and O 1s (b) peaks of 24

the zirconium oxide thin films on Si (100) as a function of substrate temperatures.

Figure 4.1.5 Valence band spectra for deposition of zirconium oxide 25

thin films on Si (100) with increased substrate temperature. The solid line indicated the edge.

Figure 4.2.1 The XRD patterns of the zirconium oxide thin films 27

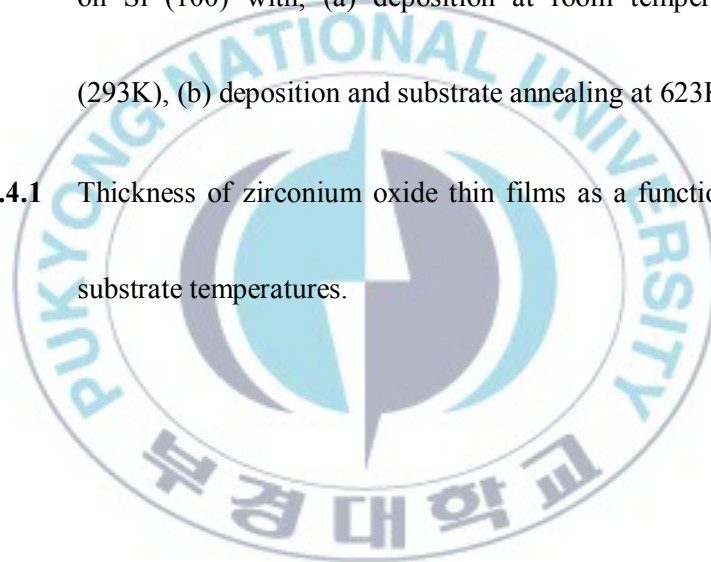
deposited on Si (100) with substrate annealing in Ar/O₂ plasma ambient. The bottom box shows the zirconium oxide of the standard JCPDS values.

Figure 4.3.1 AFM images (1μm × 1μm) of zirconium oxide thin films 29

on Si (100) with; (a) deposition at room temperature (293K), (b) deposition and substrate annealing at 623K.

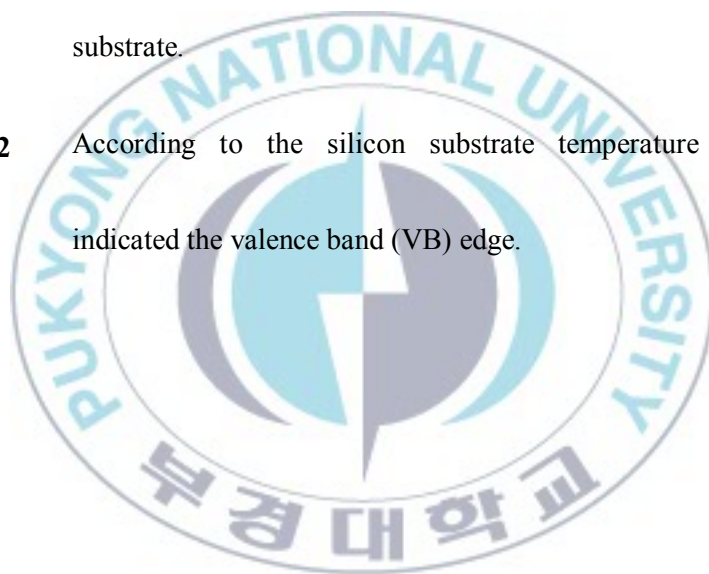
Figure 4.4.1 Thickness of zirconium oxide thin films as a function of 30

substrate temperatures.



List of Tables

Table 1	Average binding energy (BE) and full width at half maximum (FWHM) values of the zirconium oxide; Zr 3d and O 1s main peaks, as resolved from the measured Zr 3d and O 1s XPS spectra of zirconium oxide on Si (100) substrate.	20
Table 2	According to the silicon substrate temperature was indicated the valence band (VB) edge.	23



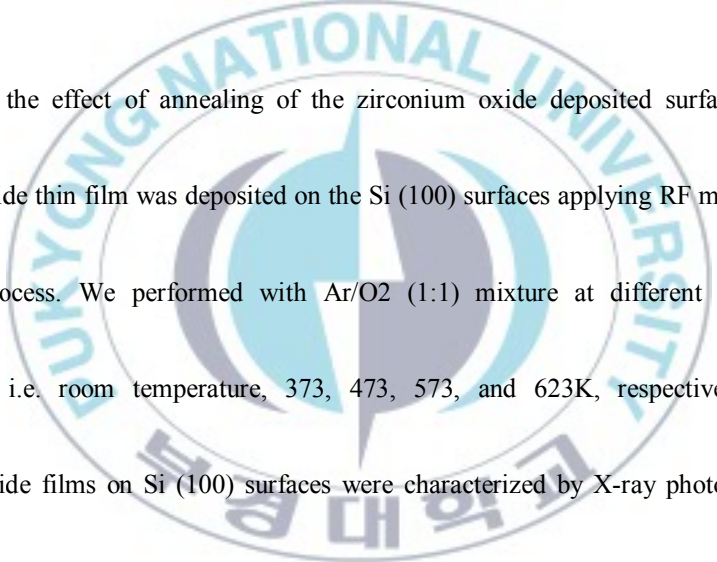
Surface phenomena of ZrO₂ coated Si (100) at different substrate temperatures

Mi sun Chun

Graduate School of Education

Pukyong National University

Abstract



We report the effect of annealing of the zirconium oxide deposited surfaces. The zirconium oxide thin film was deposited on the Si (100) surfaces applying RF magnetron sputtering process. We performed with Ar/O₂ (1:1) mixture at different substrate temperatures i.e. room temperature, 373, 473, 573, and 623K, respectively. The zirconium oxide films on Si (100) surfaces were characterized by X-ray photoelectron spectroscopy (XPS), X-ray diffraction (XRD), Atomic Force Microscopy (AFM) and spectroscopic ellipsometry (SE) techniques. The surface chemical composition and properties: a chemical shift of the Zr 3d and O 1s core levels of the zirconium oxide thin films was studied with XPS. The crystal structure of the zirconium oxide thin films was determined by XRD. The surface morphology of zirconium oxide film was investigated using AFM. The thicknesses of zirconium oxide film were indicated SE.

I . Introduction

Zirconium oxide is one of the technologically important materials characterized by a high melting point (2953 K), ionic conductivity, optical properties, good thermal insulating characteristics, high hardness, large resistance against oxidation, high refractive index, broad region of low absorption from the near-UV to the mid-IR [1,2]. In recent years there has been considerable interest in nanostructured zirconium dioxide thin films due to their potential in several applications. The combination of these properties is attractive for wide range of applications which include laser mirrors, broad band interference filters, and ionic conductors [3]. Also, Zirconium oxide thin film may be used as fuel cells [4], switchable mirrors [5], heat-resistant materials [6], optical filters [7], and sensors [8].

Zirconium oxide thin films have been widely deposited by various deposition techniques including electron-beam deposition [9], chemical vapor deposition (CVD) [10], reactive sputtering [8], radio frequency and direct current reactive magnetron sputtering [11] and ion beam sputtering deposition [12]. Most of zirconium oxide films were prepared by reactive sputtering using metal target [13]. Some zirconia

films were deposited by radio frequency (RF) sputtering with a zirconia ceramic target [14].

Advantages of zirconium oxide such as its thermal stability with Si substrate and its high dielectric constant make it one of the most promising gate dielectric candidates for SiO₂. Unfortunately, they suffer from mobility degradation, fixed charge issues [16]. Furthermore, they will crystallize at relatively low temperature, leading to the formation of grain boundaries [16-18].

In the present work, zirconium oxide thin films were deposited on p-type Si (100) wafer by RF plasma sputtering from zirconium metal target in Ar/O₂ mixed gas plasma. The resulted films were obtained at different substrate temperatures. Radio Frequency plasma sputtering has a feature that the energy and density of ions being incident into target can be controlled by RF power and matching network.

X-ray photoelectron spectroscopy (XPS) was used to study the surface chemical composition of the films. X-ray diffraction (XRD) analysis allowed lattice structure and grain size determination. Atomic force microscopy (AFM) was employed to evaluate the surface of the films morphology. And the film thickness was measured by spectroscopic ellipsometry (SE).

II . Theory

1. X-ray photoelectron spectroscopy (XPS)

X-ray photoelectron spectroscopy (XPS) is a surface chemical analysis technique that can be used to investigate the chemical environment of a material surface region. XPS is a quantitative spectroscopic technique that measures the elemental composition, chemical state and electronic state of the elements that exist within a material. For each and every element, there will be a characteristic binding energy associated with each core atomic orbital. It is each element will give rise to a characteristic set of peaks in the photoelectron spectrum at kinetic energies determined by the photon energy and the respective binding energies. The presence of peaks at particular energies therefore indicates the presence of a specific element in the sample, the intensity of the peaks is related to the concentration of the element within the sampled region. Thus, the technique provides a quantitative analysis of the surface composition and is sometimes known as electron spectroscopy for chemical analysis (ESCA).

2.1.1 Vacuum system

XPS requires ultra-high vacuum (UHV) conditions because the signal from the surface is usually very weak. All commercial spectrometers are now based on vacuum systems designed to in the UHV range of 10^{-8} Torr to 10^{-10} Torr, and it is generally accepted XPS experiment must be carried out in this pressure range. The use of UHV, in combination with sample damage which may result from irradiation with X-rays, can alter the chemical and physical structure of the film and therefore may result in inaccurate information. The need to place the sample into UHV before collecting data also removes the possibility of using XPS to measure dynamic events such as adsorption of species onto a surface.

2.1.2 X-ray source

X-ray source is used in the twin anode X-ray source or X-ray monochromator. Increased performance of monochromators, accompanied by improved sensitivity. The twin anode X-ray source is usually positioned as close to the sample as possible. The sample is therefore exposed to the radiant heat from the source region. When a monochromatic is used, this heat source is remote from the sample and thermally

induced damage is avoided. And it is possible to focus X-ray into a small spot using the monochromator. XPS can be conducted with high sensitivity.

2.1.3 XPS principle

The kinetic energy (E_K) of the electron is the experimental quantity measured by the spectrometer, but this is dependent on the photon energy of the x-rays employed and is therefore not an intrinsic material property. The binding energy of the electron (E_B) is the parameter which identifies the electron specifically, both in terms of its parent element and atomic energy level. The relationship between the parameters involved in the XPS experiment is

$$E_B = h\nu - E_K - \Phi$$

Where $h\nu$ is the photon energy, E_K is the kinetic energy of the electron, and Φ is the spectrometer work function.

As all three quantities on the right hand side of the equations are known or measurable, it is a simple matter to calculate the binding energy of the electron. In practice, this task will be performed by the control electronics or data system associated with the spectrometer and the operator merely selects a binding or kinetic

energy scale.

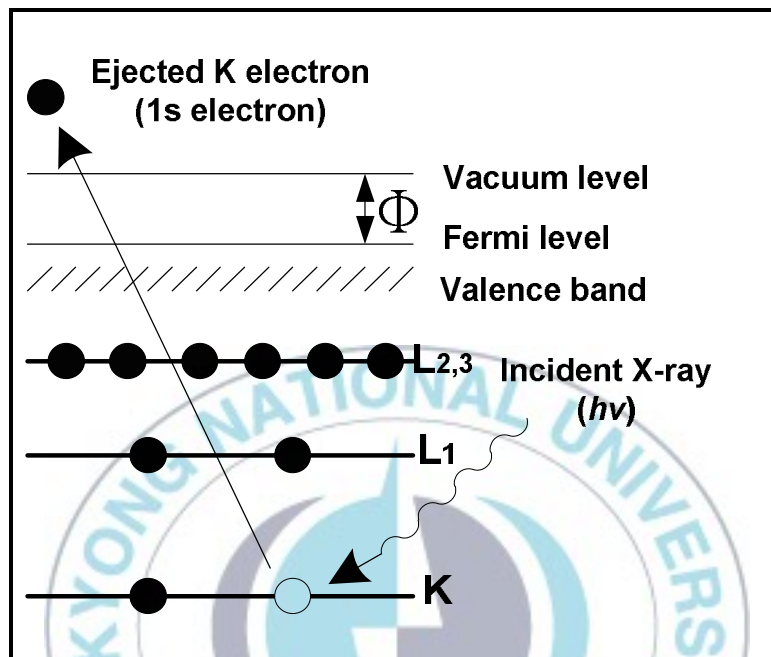


Figure 2.1.1 Schematic diagram of the XPS process, showing photoionization of an atom by the ejection of a 1s electron.

2.1.4 Photoemission process

The process of photoemission is shown schematically in Figure 2.1 where an electron from the K shell is ejected from the atom (a 1s photoelectron) by incident X-ray source. The photoelectron spectrum will reproduce the electronic structure of an

element quite accurately since all electrons with a binding energy less than the photon energy will feature in the spectrum. Those electrons which are excited and escape without energy loss contribute to the characteristic peaks in the spectrum which inelastic scattering and suffer energy loss contribute to the background of the spectrum. Once a photoelectron has been emitted, the ionized atom must relax in some way.

The other possibility is the ejection of an Auger electron after the core hole is produced. Thus Auger electrons are produced as a consequence of the XPS process often referred to as X-AES (X-ray induced Auger electron spectroscopy). X-AES, although not widely practiced, can yield valuable chemical information about an atom. For the time being we will restrict our thoughts to AES in its more common form, which is when a finely focused electron beam causes the emission of Auger electrons.

III. Experiment

3.1 Experimental apparatus and procedure

Zirconium oxide films were deposited on p-type Si (100) wafer substrates by reactive RF magnetron sputtering from a metallic zirconium target with a diameter of 50 mm and a thickness of 3 mm. The Si substrates with native oxide were carefully cleaned by ultrasonic bath in high purity ethanol (99.9%) for 5 min, and dried under flowing N₂ gas [3]. Before deposition, the vacuum chamber was evacuated using a roughing pump (RP) to 2.0×10^{-5} Torr and a turbo molecular pump (TMP) to 1.0×10^{-7} Torr. The sputtering gas Ar with a high purity of 99.99% and the reactive gas O₂ with a high purity of 99.99% were introduced to chamber separately and controlled by standard mass flow controllers.

The zirconium target was cleaned by pre-sputtering with an RF power (13.56 MHz) of 20 W for 1 hr with high purity Ar gas and the substrate was shielded with a shield in order to remove the surface contaminants on the target and stabilize the sputtering.

In the present work, sputtering was performed at different substrate temperatures with the same RF power of 20 W for 3 hr. The pressure of the sputtering chamber

during the RF sputtering process was kept at 1.5×10^{-5} Torr as measured by a cold cathode gauge. During the sputtering, the flow gases in an Ar/O₂ (1:1) mixture and keeping constant the total gases flowing flux at 20 sccm. The zirconium films were deposited at different substrate temperatures i.e. room temperature, 373, 473, 573, and 623 K, respectively.

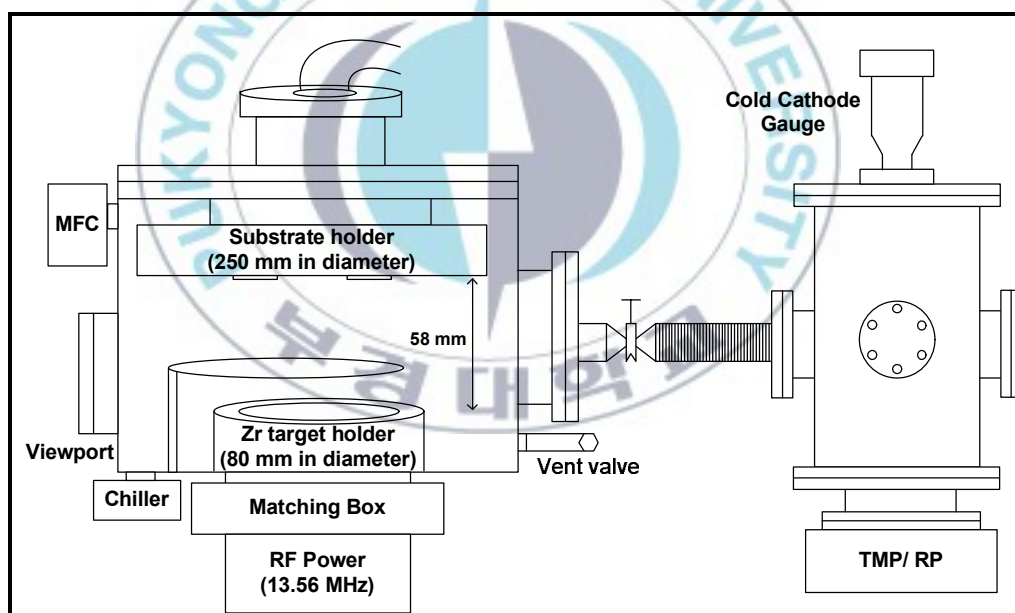


Figure 3.1.1 Schematic representation of RF magnetron sputtering chamber.

3.2 Instrumental analysis of Zirconium oxide thin films

3.2.1 The experimental condition of XPS

The compositional analysis zirconium oxide thin film was analyzed by XPS (VG ESCALAB 2000), using an Al K α X-ray source (1486.6 eV). The XPS chamber was pumped by two stages of pumping system. The first one is that a TMP backed by a two stage RP system pumps. And the second system consists of an ion getter pump and a Ti-sublimation pump and evacuates analysis chamber to maintain UHV condition. X-ray source was at high voltage of 15.0 kV, beam current of 16.5 mA, and filament current of 1.6 A. The survey XP spectra were collected in a concentric hemispherical analyzer (CHA) in constant analyzer energy (CAE) mode with a pass energy of 50 eV, a dwell time of 50 ms, and an energy step size of 0.5 eV. The base pressure in the analysis chamber was maintained at about 7.5×10^{-9} Torr or lower. The binding energy (BE) scale was calibrated by using the peak of adventitious carbon, setting it to 284.6 eV [24]. High resolution spectra were obtained at a pass energy of 20 eV, an energy step size of 0.05 eV steps and other factors were kept the same as those applied in the survey scan.

3.2.2 Deconvolution of Zr 3d and O1s

High resolution spectra were deconvoluted using XPSPEAK software (ver 4.1) for data analysis in order to more accurately determine the binding energy of core level electron of the different elements. Obtained XPS C 1s, Zr 3d, and O 1s peaks were divided into several peaks according to their chemical environments. As a Shirley-type background subtraction, the spectra were fitted using a Gaussian-Lorentzian peak shape. The full width half maximums (FWHM) of C 1s, Zr 3d and O 1s peak were 1.398~1.41 eV, 1.084~1.2 eV, and 1.368~1.624 eV, respectively the G/L ratio was 30% (Lorentzian – 30%, Gaussian – 70%) and the spin-orbit splitting (SOS) constant for Zr 3d was 2.4 eV [19,22].

3.2.3 The experimental condition of XRD

The crystal structure of the zirconium oxide thin films deposited on Si (100) wafer was determined by X-ray diffraction (XRD) using a PHIIPS (Netheland) X`Pert-MPD system applying grazing mode. The used X-ray source was Cu K α radiation at the wavelength of 1.54056 Å. The current and voltage for the measurement were 30 mA and 40 kV, respectively. The scanning angle 2 θ was varied from 10° to 80° with a

detection step of 0.02° . Grazing incidence measurements are very sensitive to the structure of the thin films. The incidence angle is sufficient to collect all information from the sample under investigation. The JCPDS international diffraction data base [20] has been used to indentify the crystalline phase.

3.2.4 The experimental condition of AFM and SE

The surface morphology of zirconium oxide film was investigated using atomic force microscopy (AFM), a Veeco Multimode Digital Instruments Nanoscope III α system, in contact mode. The surface roughness was measured as root mean square (RMS) value over the area of $1\mu\text{m} \times 1\mu\text{m}$.

The thickness of the zirconium oxide thin films was deduced by spectroscopic ellipsometry (SE), gaertner L2W830 ellipsometer. SE measurements were performed at incident angles of 70° and wavelength of 6328 nm. The index of refraction was fitting with 2.17 for zirconium oxide constant.

IV. Results and Discussion

4.1 X-ray photoelectron spectroscopy of Zirconium oxide

Figure 4.1.1 shows survey scan of X-ray photoelectron spectroscopy zirconium oxide (ZrO_2) on Si (100) wafer in the binding energy range of 0~1300 eV. The bottom spectrum was pure silicon wafer. The second spectra from the bottom shows the spectra after zirconium oxide thin films were deposited on Si (100) using RF plasma sputtering of the zirconium target and Ar/O_2 (1:1) mixture. Before deposition, the bare Si substrate is presented at Si 2s (150.5 eV) and Si 2p (99.5 eV) [19,21]. After zirconium oxide deposition at different substrate temperatures, spectra show that Zr 3s (432.4 eV), Zr 3d (182.0 eV, 184.4 eV), Zr 3p (346, 322 eV) and Zr 4p (30.8 eV) [22,23]. The native oxide and carbon are presented at O 1s (530 eV) and C 1s (284.6 eV) [24]. Auger peaks are indicated for O (KLL) and C (KLL) [25].

The peak intensity of Zr 3d was increased with increasing substrate temperature of zirconium oxide deposition. Also, the peak intensity of O 1s was increased as well. It is clear that zirconium oxide films were coated on silicon substrate.

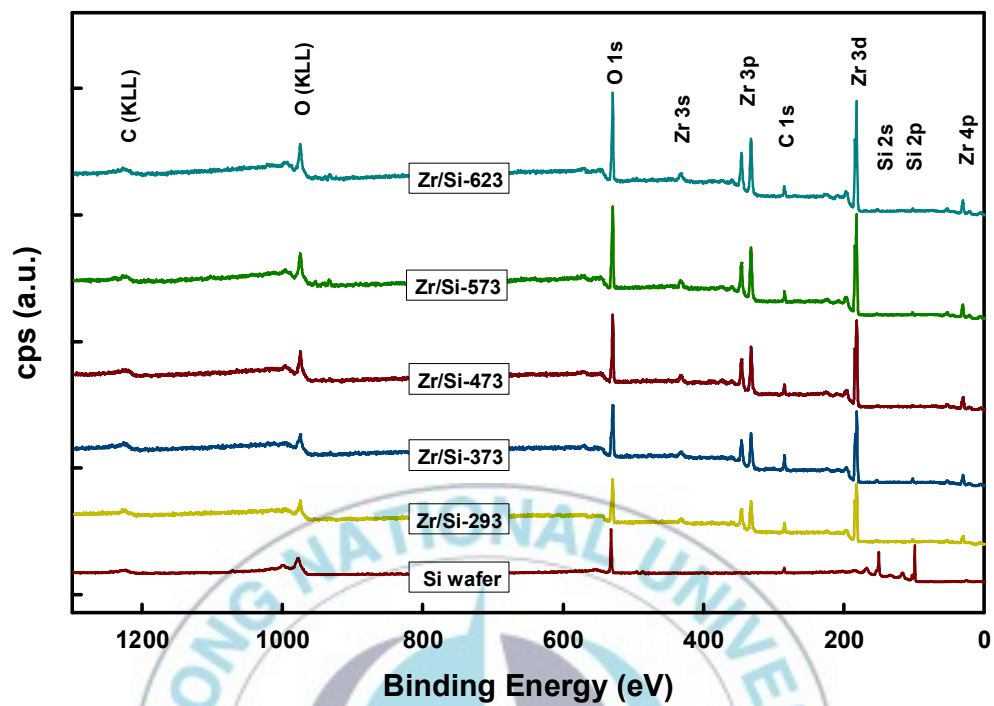


Figure 4.1.1 The survey XPS of zirconium oxide on Si (100) before and after zirconium oxide deposition and substrate annealing.

Figure 4.1.2 (a) shows the Zr 3d core level XPS spectra. Before substrate heating at room temperature (293K), there is a doublet peaks were observed corresponding to Zr $3d_{5/2}$ and Zr $3d_{3/2}$ features at 181.9 eV and 184.3 eV, respectively, which were separated by 2.4 eV, the magnitude of spin-orbit splitting constant. After substrate heating (623 K), the binding energies were 182.1 eV and 184.5 eV for $3d_{5/2}$ and $3d_{3/2}$ levels, which was shifted by about 0.2 eV from the peaks obtained at 293 K [22]. A peak shift to slightly higher binding energy was observed. It may be due to the production of zirconium oxide as increased the substrate temperature. This could be explained by considering complete oxidation of zirconium to zirconia in its +4 oxidation state [21,23,26]. But when the substrate heated up to 473 K, the peaks of $3d_{5/2}$ and $3d_{3/2}$ were 181.8 eV and 184.2 eV, respectively. The peaks were shifted back to lower binding energy. This might indicate bonding between Zr-Si states [38].

The deconvoluted high resolution XP spectra of the Zr 3d at 293 and 623 K are shown in Figure 4.1.2 (c) and Figure 4.1.2 (b), respectively. The Zr 3d spectra can be curve-fitted with three peaks: zirconia (ZrO_2), zirconium with higher (ZrO_x : $0 < x < 2$) and lower oxidation state (ZrO_y : $0 < y < 2$, $x > y$) [28]. The Zr 3d of zirconium oxide is centered at 182.1 eV, Zr 3d of higher oxidation state is centered at 182 eV, and Zr 3d

of lower oxidation state is centered at 181.5 eV. As increased substrate temperature the oxidation state of higher and lower oxidation state were changed to zirconia. According to these results, we can confirm that the higher substrate temperature produced more than zirconia on the thin films deposited on the silicon substrate.



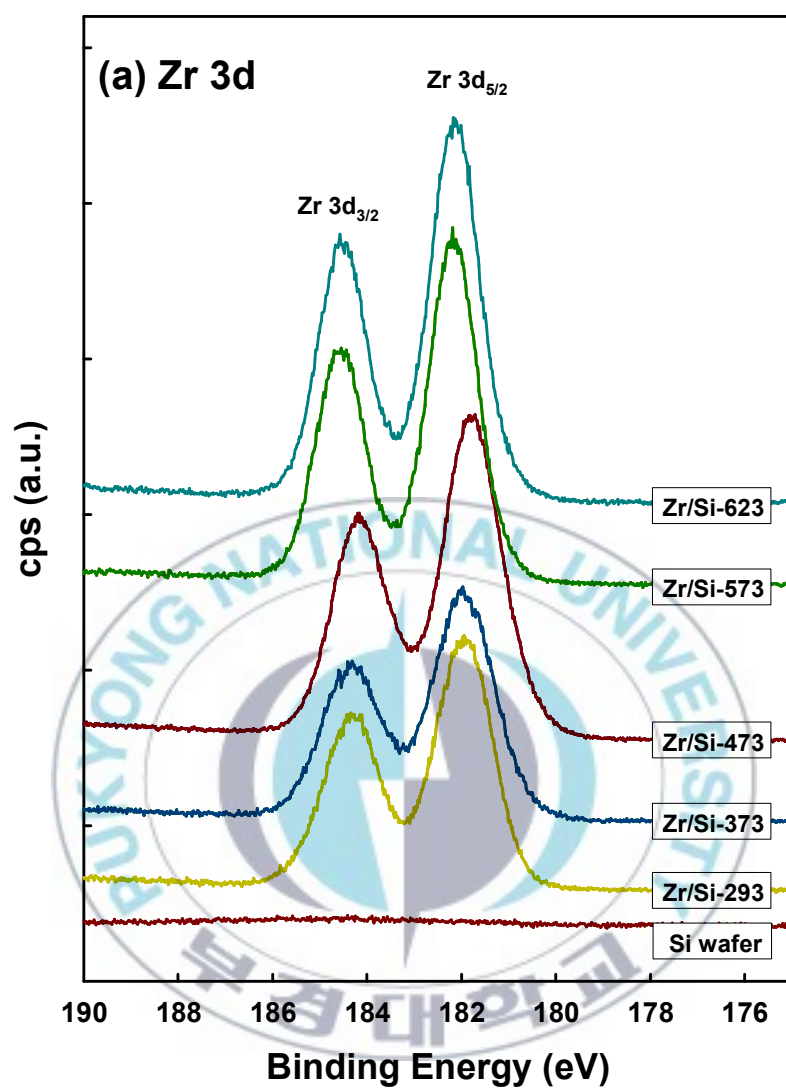


Figure 4.1.2 (a) stacked XP spectra of the Zr $3d_{5/2}$ and $3d_{3/2}$ which zirconium oxide thin film on Si (100) with increased substrate temperature.

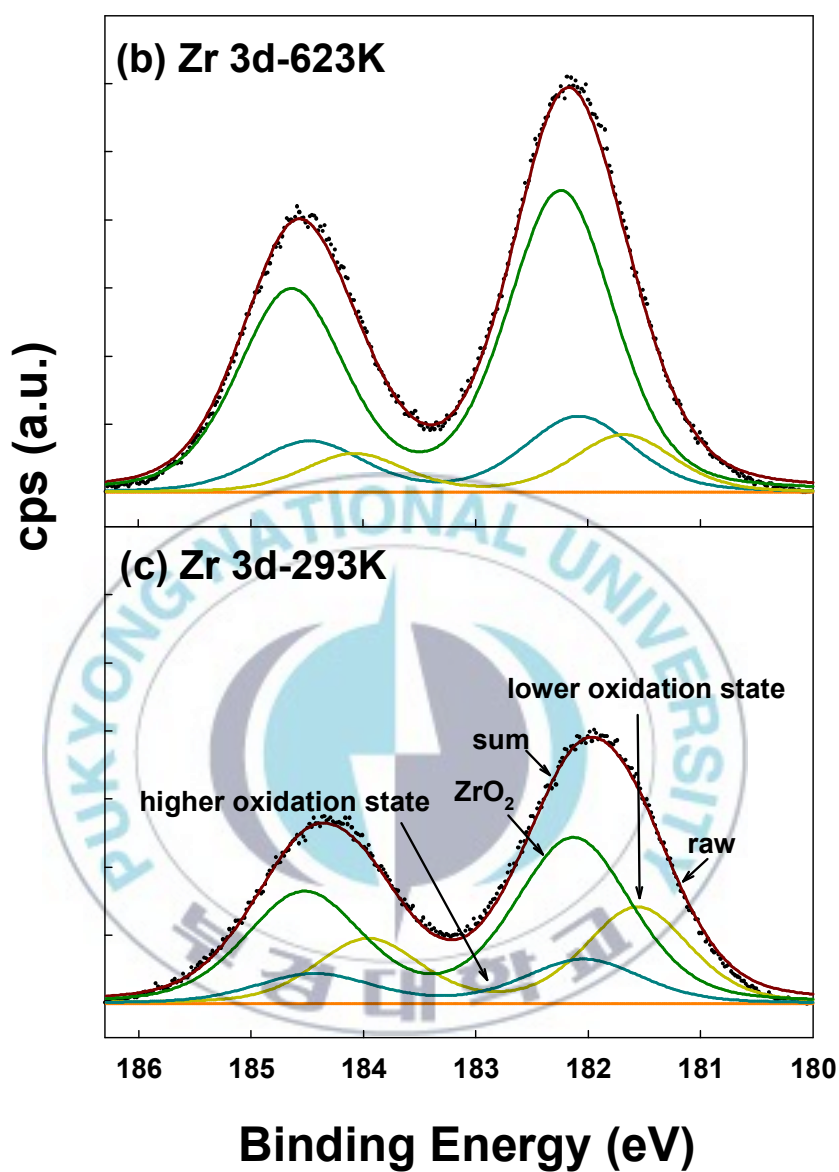


Figure 4.1.2 Deconvoluted XP spectra of the Zr 3d when silicon substrate temperature at 623K (b) and 293K (c). The Zr 3d spectrum was separated three oxidation state; zirconia (ZrO_2), higher oxidation state and lower oxidation state. The spots represent raw data, smooth lines mean sum of deconvoluted Zr 3d.

The representative O 1s XPS spectra of zirconium oxide thin film on silicon substrate at different substrate temperatures were stacked in Figure 4.1.3 (a). Before zirconium oxide deposited on the silicon wafer, the silicon dioxide (SiO_2) peak appeared to 531.7 eV [19]. After zirconium oxide deposited on Si (100), the zirconium oxide (Zr-O) peak indicated at 529.6 eV [30]. As increasing substrate temperature, O 1s peak intensity was increased. Comparison with Figure 4.1.2 (a), the peak position of O 1s shifted 0.2 eV. The shift of peaks Zr 3d and O 1s signify that those oxidation states were changed. For the heating zirconium oxide thin films may cause to partial bonding of zirconium atoms with the oxygen.

The comparison of high resolution XP spectra of the O 1s region at 623 K and 293 K are shown in Figure 4.1.3 (b) and Figure 4.1.3 (c). The O 1s spectra were decomposed with four peaks; zirconia (ZrO_2), higher and lower oxidation state (ZrO_x , ZrO_y), surface oxygen (-OH), and silicon dioxide (SiO_2). The O 1s peak of silicon dioxide (SiO_2) is centered at 532.4 eV, surface oxygen is centered at 531.7 eV, higher and lower oxidation state (ZrO_x , ZrO_y) is centered at 530 eV, and zirconia (ZrO_2) is centered at 529.5 eV. The best fitting parameters are given in Table 1.

There was similarity with the Figure 4.1.2 (b) and (c). The zirconium with higher and lower oxidation state was altered to the zirconia. The oxidation state of zirconium change and be stabilized on silicon substrate by increased substrate temperature.

Component	BE (eV)	FWHM (eV)
Zr 3d main peak		
Lower oxidation state (ZrO_y)	181.55 ± 0.17	1.08 ± 0.08
Higher oxidation state (ZrO_x)	182.00 ± 0.15	1.20 ± 0.10
Zirconia (ZrO_2)	182.15 ± 0.13	1.17 ± 0.09
O 1s main peak		
Zirconia (ZrO_2)	529.54 ± 0.19	1.37 ± 0.01
Higher and lower oxidation state ($\text{ZrO}_{x,y}$)	530.00 ± 0.06	1.62 ± 0.03
Surface oxygen (-OH)	531.70 ± 0.12	1.42 ± 0.01
Silicon dioxide (SiO_2)	532.41 ± 0.06	1.39 ± 0.02

Table 1 Average binding energy (BE) and full width at half maximum (FWHM) values of the zirconium oxide; Zr 3d and O 1s main peaks, as resolved from the measured Zr 3d and O 1s XPS spectra of zirconium oxide on Si (100) substrate.

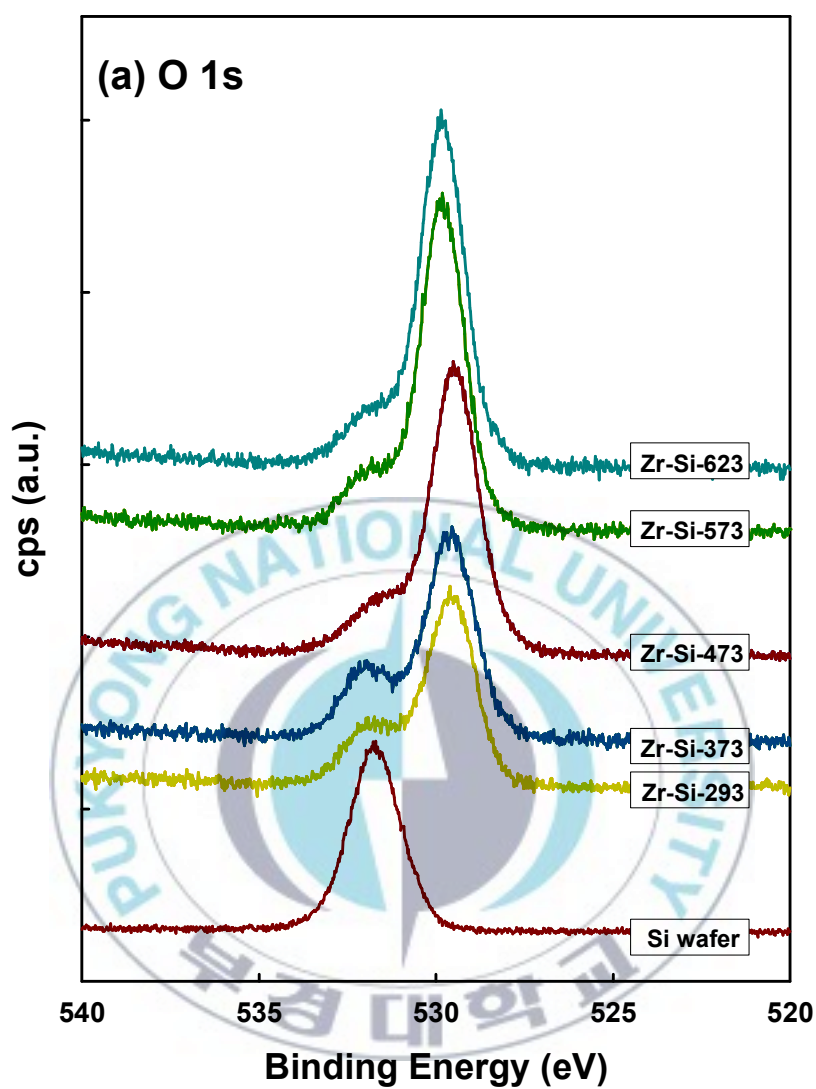


Figure 4.1.3 (a) XP spectra of the O 1s region zirconium oxide on Si (100) with different substrate heating temperature. The silicon dioxide (SiO₂) peak was assigned at 531.7 eV, and the zirconium oxide (Zr-O) was assigned at 529.6 eV.

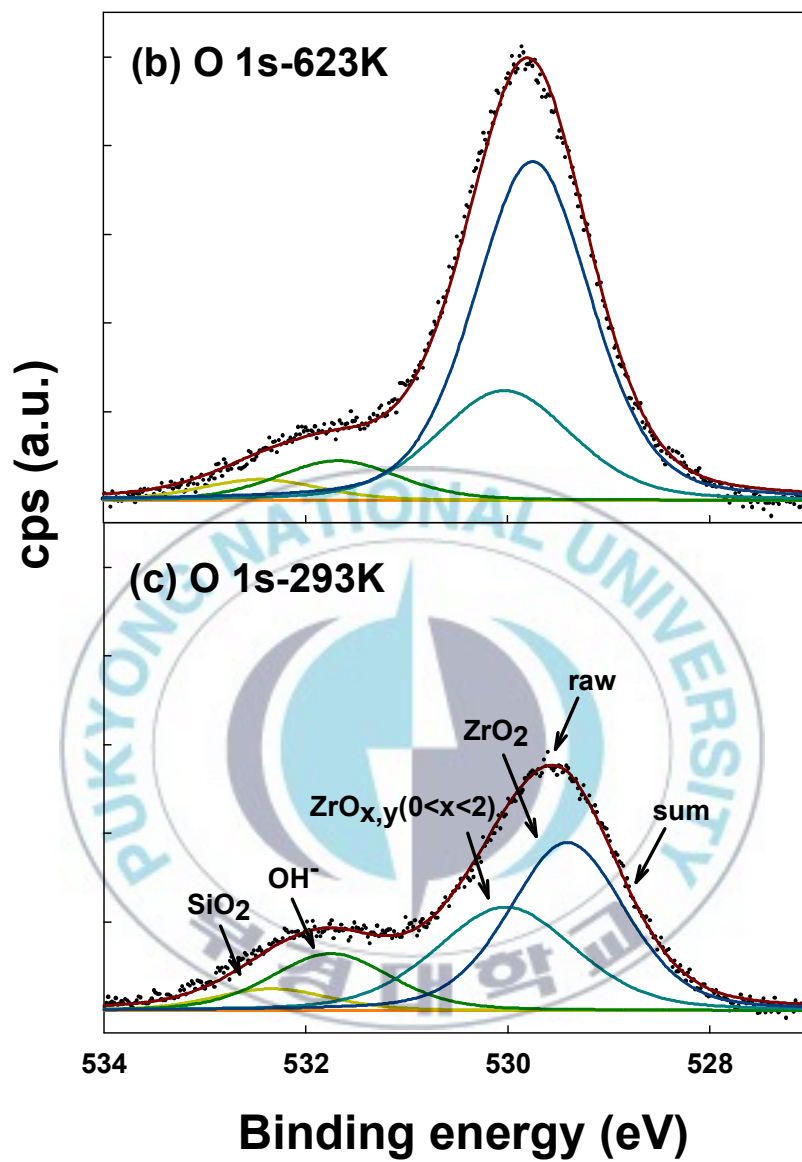


Figure 4.1.3 Deconvoluted XP spectra of the O 1s when silicon substrate temperature was 623 K (b) and 293 K (c). The O 1s spectra were separated four oxidation state; zirconia (ZrO_2), higher and lower oxidation state ($\text{ZrO}_{x,y}$), surface oxygen ($-\text{OH}$), silicon oxide (SiO_2). The bottom solid lines are background.

The integrated area ratios of Zr 3d and O 1s in different chemical environments with different substrate temperatures Figure 4.1.4 (a) and (b), respectively. There were showed zirconium oxide of the higher and lower oxidation state (ZrO_x , ZrO_y) changed to the zirconia (ZrO_2) as increasing substrate temperature. This consequence was well consistent with the XP spectra of Zr 3d and O 1s indicated.

Figure 4.1.5 shows the valence band spectra of zirconium oxide thin films coated on Si (100). The silicon substrate valence band was dominated mainly by the Si 3s and Si 3p orbitals extending from approximately 7 eV and 1.5 to 4.5 eV [37]. When the zirconium oxide on silicon the valence band spectra was confirmed at around 4.5 to 7 eV [31,32]. This result could be assigned to surface zirconium oxide which the peak was supposed Zr 4d (6.7 eV) and O 2p (5 eV) orbitals overlap [24,39].

The valence band (VB) edge showed with different substrate temperatures in Table 2. In each of the spectra, the onset of the binding energy was determined by extrapolating the segment and linear least squares method. It is considered to the data obtained in this way, as increasing the substrate temperature was increasing the valence band edge. At the substrate temperature of 473 K, however, valence band edge was decreased. This result was supported by XPS result explained it previously

XP spectra of the Zr 3d and O 1s was indicated that peaks was shifted to lower binding energy substrate temperature at 473 K. This result shows that Zr-Si interface signal was appeared to lower binding energy [38]. It could be estimated that thickness of zirconium oxide thin film was comparative thinner than others. This prediction spectroscopic ellipsometry (SE) data can be found it.

Substrate temperature (K)	VB edge (eV)
293	2.280
373	2.513
473	2.098
573	2.680
623	2.724

Table 2 According to the silicon substrate temperature was indicated the valence band (VB) edge.

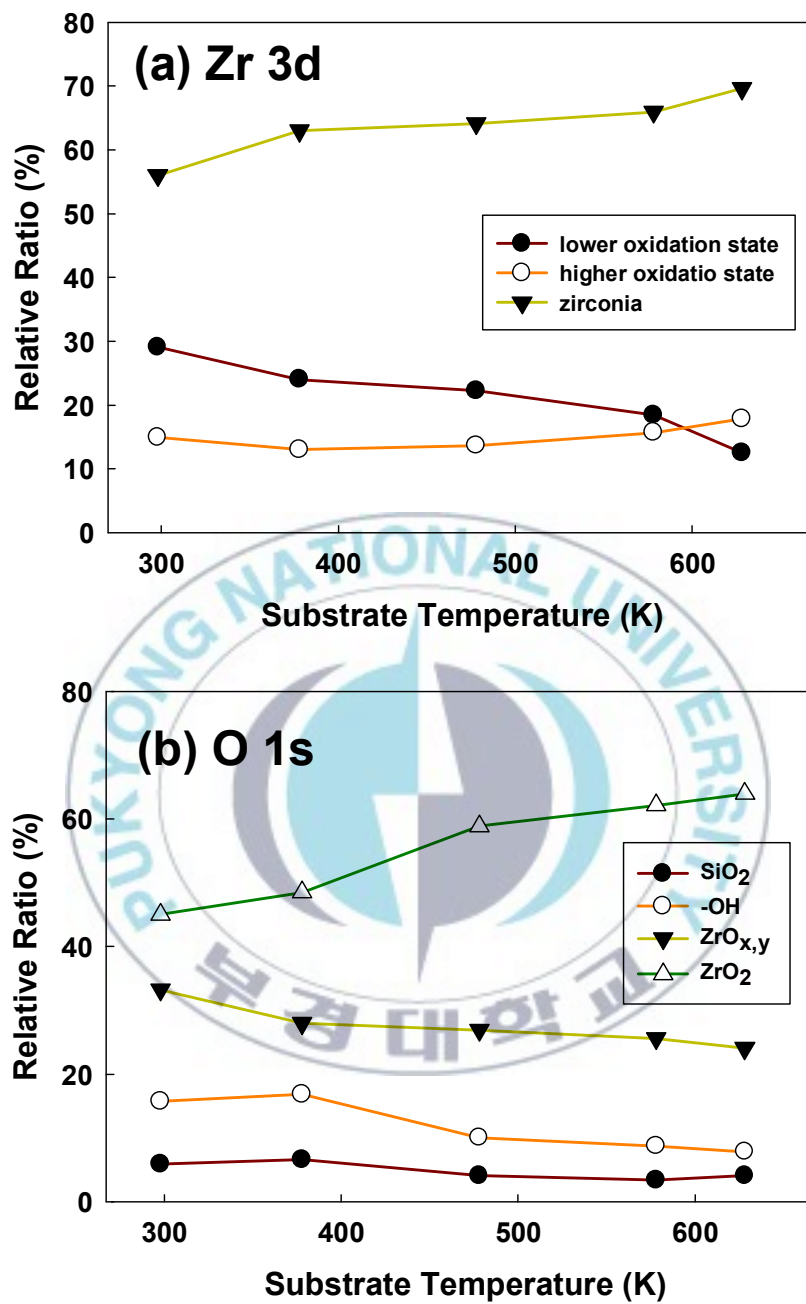


Figure 4.1.4 The relative ratios of the Zr 3d (a) and O 1s (b) peaks of the zirconium oxide thin films on Si (100) as a function of substrate temperatures.

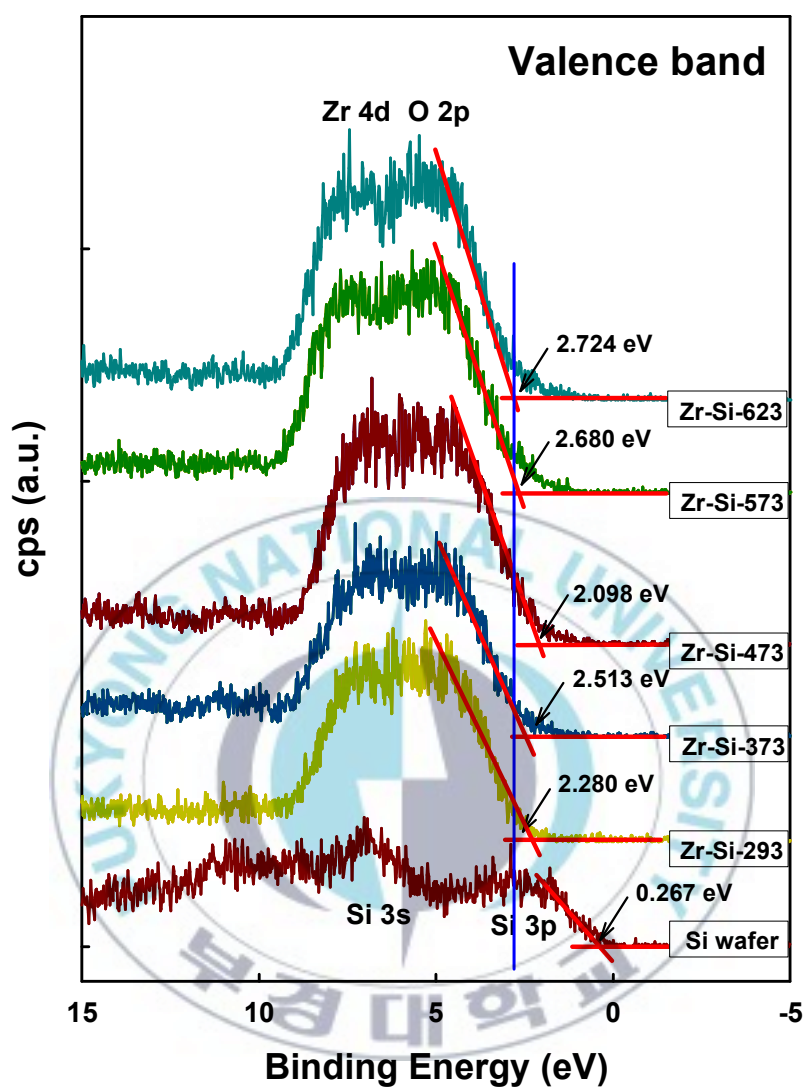


Figure 4.1.5 Valence band spectra for deposition of zirconium oxide thin films on Si (100) with increased substrate temperature. The solid line indicated the edge.

4.2 X-ray diffraction of Zirconium oxide

The crystallized structures of the zirconium oxide thin films deposited in various substrate temperatures are shown in Figure 4.2.1. It has been reported that zirconium oxide exists in three different crystalline phases. The monoclinic phase is stable up to 1443 K, a tetragonal phase is reported between 1443 K and 2643 K and finally a cubic phase exists up to the melting point 3133 K [33,34]. The XRD measurements reveal that the monoclinic phase has formed without any phase mixing. The diffraction peaks were indexed according to standard JCPDS patterns for zirconia (ZrO_2) lattice [20].

The zirconium oxide thin films were deposited on Si (100) with increased substrate temperature in Ar/O_2 plasma conditions. Before substrate heating, the zirconium oxide films show a very weak diffraction peak for monoclinic (-111) and (100). Since 573 K of the substrate temperature there is an increase in the intensity of (202) peak for monoclinic phase. The diffusion of oxygen through the zirconium oxide films is enhanced under high deposition temperature, as zirconium oxide films have been previously reported to be an oxygen ion conductor and have high oxygen diffusivity [35].

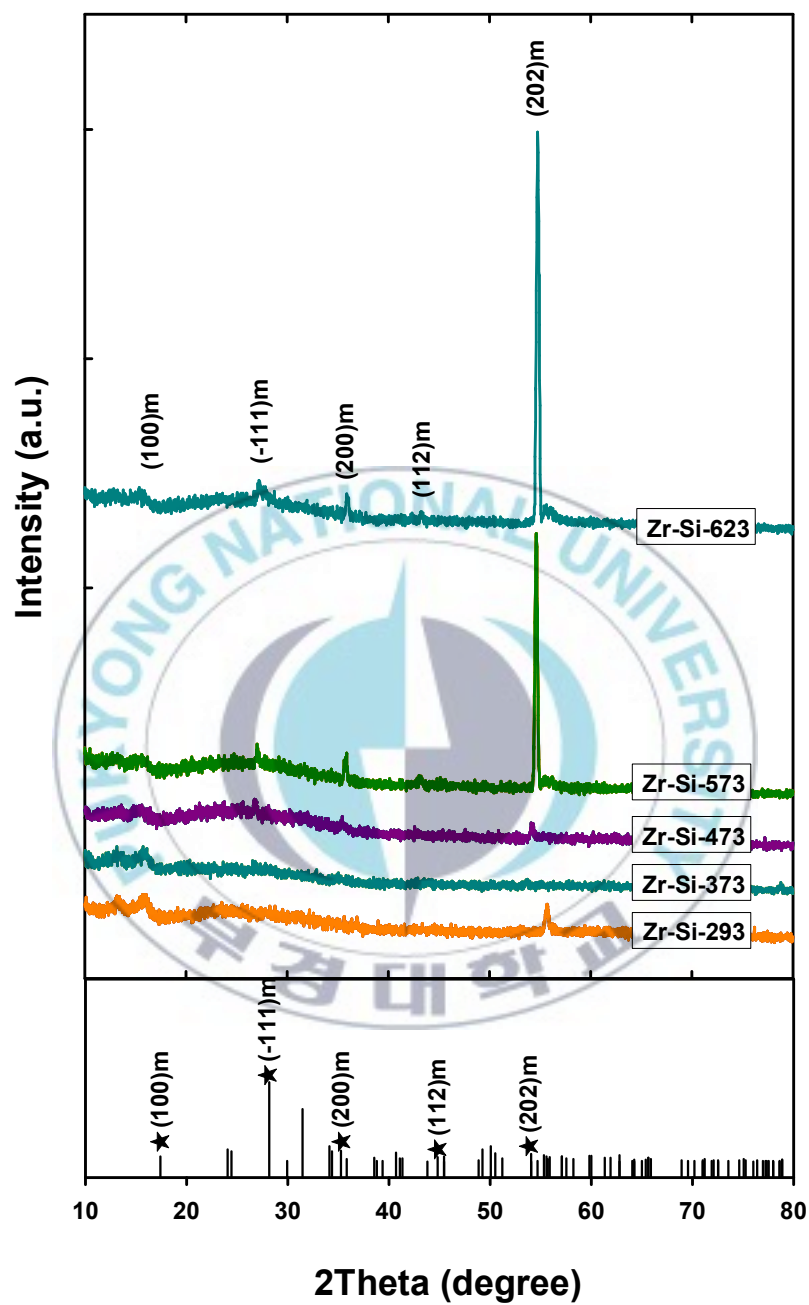


Figure 4.2.1 The XRD patterns of the zirconium oxide thin films deposited on Si (100) with substrate annealing in Ar/O₂ plasma ambient. The bottom box shows the zirconium oxide of the standard JCPDS values.

4.3 Atomic force microscopy of Zirconium oxide

Figure 4.3 show representative AFM images of zirconium oxide thin films coated on Si (100) at different substrate temperature in contact mode. Figure 4.3 (a) presents the surface morphology of thin films deposited at room temperature. This film has a RMS roughness of 2.42 nm. Figure 4.3 (b) shows the zirconium oxide thin films with the substrate temperature of 623 K, its RMS roughness is 0.23 nm.

As the substrate temperature increased, RMS values are decreased significantly and formed a more regular films surface. Obviously the surface morphology of the film deposited at 623 K is smoother than that of deposited at room temperature. This result could make certain of the zirconium oxide thin films roughness decreased by increasing substrate temperature. With increasing the substrate temperature, the RMS values decreased, which means that the substrate temperature has significant effects on the surface roughness [36].

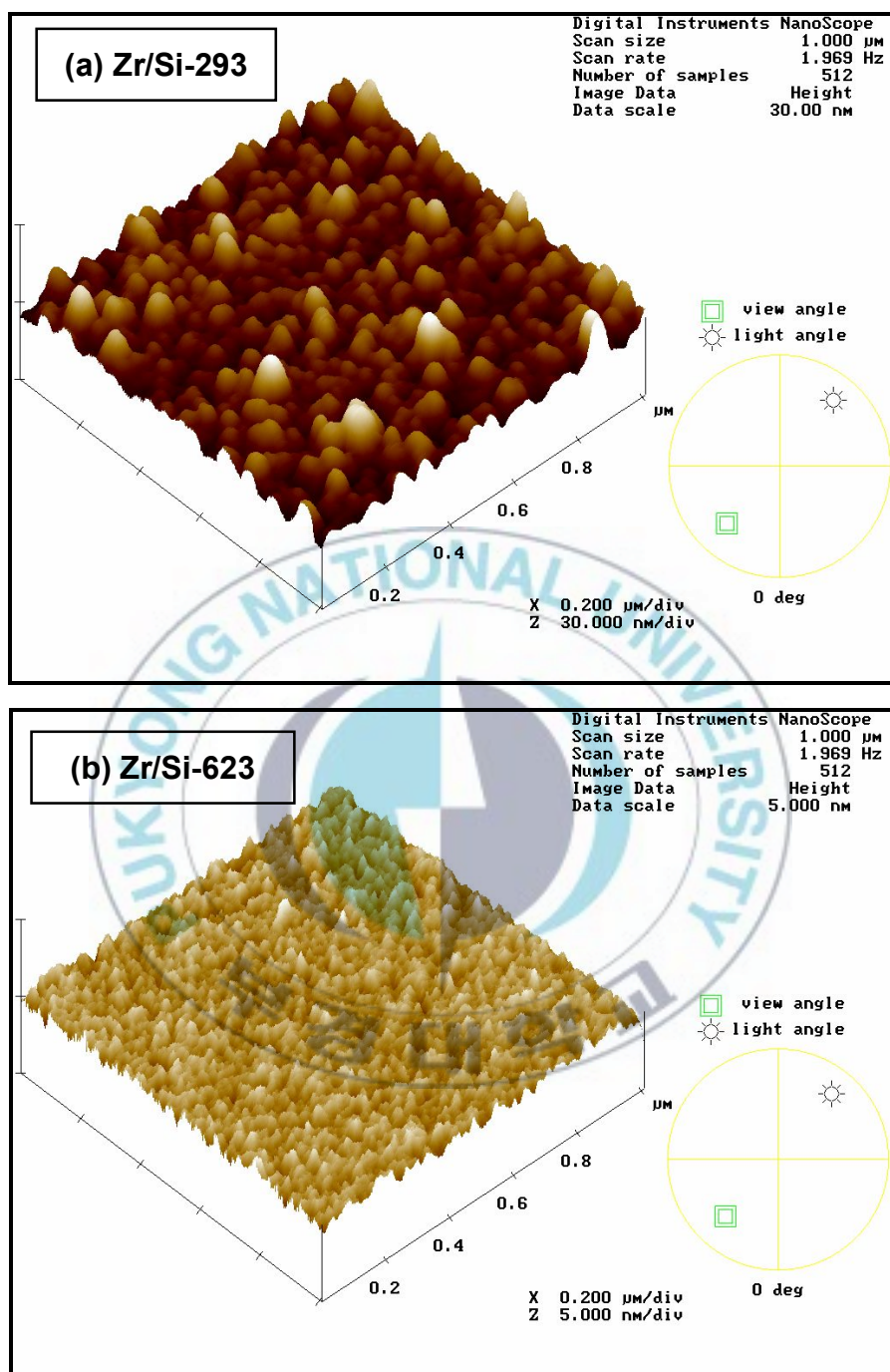


Figure 4.3.1 AFM images ($1\mu\text{m} \times 1\mu\text{m}$) of zirconium oxide thin films on Si (100)

with; (a) deposition at room temperature (293 K), (b) deposition and substrate annealing at 623 K.

4.4 Spectroscopic ellipsometry of Zirconium oxide

Figure 4.4.1 shows the thickness of zirconium oxide thin films formed at different substrate temperatures measured by SE technique. The thicknesses of these films were relatively constant. But, there was a slight decrease in zirconium oxide thin films thickness with the increase of substrate temperature. It may be due to the increased packing density and increased evaporation effects of the surface atoms at high temperature.

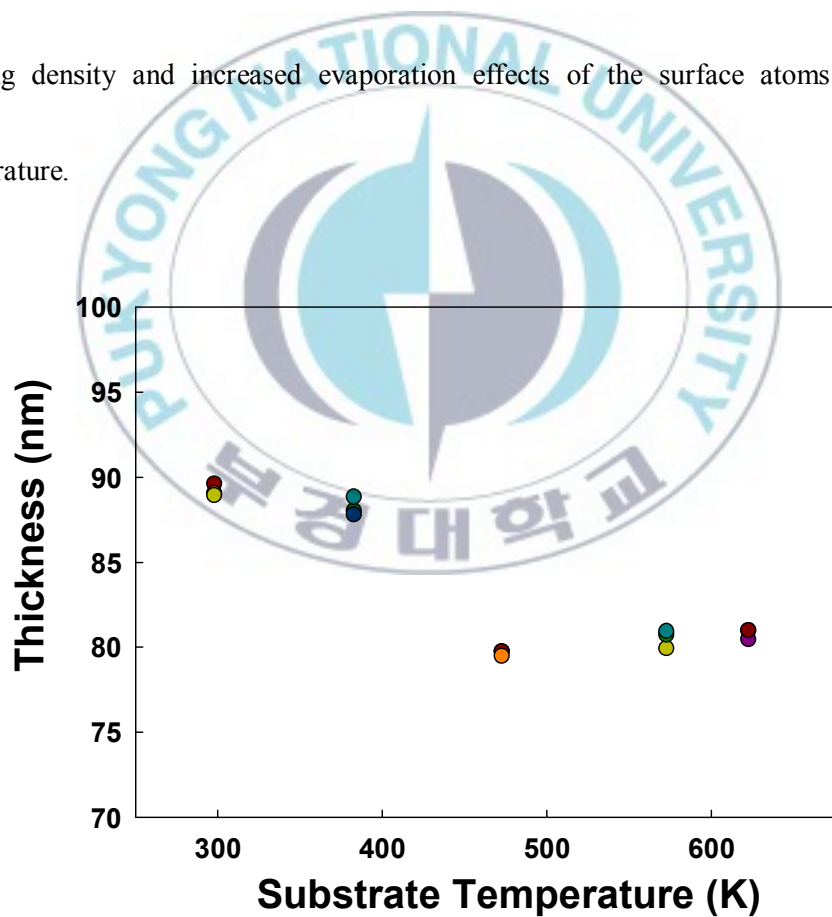


Figure 4.4.1 Thickness of zirconium oxide thin films as a function of substrate temperatures.

V. Conclusion

Zirconium oxide thin films were deposited on p-type Si (100) with different substrate temperature in Ar/O₂ (1:1) plasma mixture applying radio frequency (RF) magnetron sputtering process. The zirconium oxide thin films surfaces were characterized by X-ray photoelectron spectroscopy (XPS), X-ray diffraction (XRD), Atomic Force Microscopy (AFM), and spectroscopic ellipsometry (SE) techniques.

The XPS confirmed that the change ZrO_x, ZrO_y (lower and higher oxidation state) to ZrO₂ (zirconia) with increasing the substrate temperature. The XRD indicates the zirconium oxide forms a monoclinic crystal at 578 K. The AFM image shows the roughness decreased by increasing the substrate temperature. The surface of thickness was comparative constant obtained by SE.

VI. References

- [1] S. Venkataraj, O. Kappertz, H. Weis, R. Drese, R. Jayavel, and M. Wuttig, J. Appl. Phys. 92 (2002) 3599.
- [2] P. T. Gao, L. J. Meng, M. P. dos Santos, V. Teixeira, and M. Andritschky, Vacuum 56 (2000) 143.
- [3] C. Y. Ma, F. Lapostolle, P. Briois, and Q. Y. Zhang, Appl. Surf. Sci. 53 (2007) 8718.
- [4] C. D. Baertsch, K. F. Jensen, J. L. Hertz, H. L. Tuller, S. T. Vengallatore, S. M. Spearing, and M. A. Schmidt, J. Mater. Res. 19 (2004) 2604.
- [5] A. L. Larsson and A. G. Niklasson, Sol. Energ Mater. Sol. Cells 84 (2004) 351.
- [6] N. Q. Minh, J. Am. Ceram. Soc. 76 (1993) 563.
- [7] A. Feldman, X. Yang, and E. N. Farabaugh, Appl. Opt. 28 (1989) 5229.
- [8] D. H. Kuo and C.H. Chen, Thin Solid Film 429 (2003) 40.
- [9] K. Wada, N. Yamaguchi, and H. Matsubara, Surf. Coat. Technol. 184 (2004) 55.
- [10] J. Jeong and K. Yong, J. Cryst. Growth 254 (2003) 65.
- [11] P. F. Carcia, R. S. McLean, M. H. Reilly, Z. G. Li, L. J. Pillione, and R. F.

- Messier, J. Vac. Sci. Technol. A 21 (2003) 745.
- [12] H. K. Pulker, Surf. Coat. Technol. 112 (1999) 250.
- [13] L. S. Wang and S. A. Barnett, J. Electrochem. Soc. 139 (1992) 1134.
- [14] M. Hartmanova, K. Gmucova, and I. Thurzo, Solid State Ionics 130 (2000) 105.
- [15] G. D. Wilk, R. M. Wallance, and J. M. Anthony, J. Appl. Phys. 89 (2001) 5243.
- [16] G. He, Q. Fang, M. Liu, L. Q. Zhu, and L. D. Zhang, J. Cryst. Growth 268 (2004) 155.
- [17] J. M. Howard, V. Cracium, V. Essary, and R. K. Singh, Appl. Phys. Lett. 81 (2002) 3431.
- [18] L. Q. Zhu, G. He, M. Liu, Q. Fang, and L.D. Zhang, Mater. Lett. 60 (2006) 888.
- [19] C. D. Wagner, W. M. Riggs, L. E. Davis, J. F. Moulder, and G. E. Muilenberg (Ed.), Handbook of X-ray photoelectron spectroscopy. (1992) p100.
- [20] JCPDS Database, International Center for Diffraction Data. (2003) PDF 83-0940.
- [21] Y. -M. Sun, J. Lozano, H. Ho, H. J. Park, S. Veldman, and J. M. White, Appl. Surf. Sci. 161 (2000) 115.

- [22] G. Cabillo, L. Lillo, C. Caro, G. E. Buono-Core, B. Chornik, and M. A. Soto, J. Non-Cryst. Solids 354 (2008) 3919.
- [23] N. L. Zhang, Z. T. Song, Q. Wan, Q. W. Shen, and C. L. Lin, Appl. Surf. Sci. 202 (2002) 126.
- [24] I. Espitia-Cabrera, H. D. Orozco-Hernandez, P. Bartolo-Perez, and M. E. Contreras-Garcia, Surf. Coat. Technol. 203 (2008) 211.
- [25] Y. Ohtsu, M. Ehami, H. Fujita, and K. Yukimura, Surf. Coat. Technol. 196 (2005) 81.
- [26] T. S. Jeon, J. M. White, and D. L. Kwong, Appl. Phys. Lett. 78 (2001) 368.
- [27] A. Lyapin, L. P. H. Jeurgens, and E. J. Mittemeijer, Act. Mater. 53 (2005) 2925.
- [28] W. -J. Qi, R. Nieh, B. H. Lee, L. Kang, Y. Jeon, and J. C. Lee, Appl. Phys. Lett. 77 (2000) 3269.
- [29] T. S. Jeon, J. M. White, and D. L. Kwong, Appl. Phys. Lett. 78 (2001) 368.
- [30] L. Q. Zhu, Q. Fang, G. He, M. Liu, X. X. Xu, and L. D. Zhang, Mater. Sci. Semicond. Pro. 9 (2006) 1025.
- [31] S. Miyazaki, M. Narasaki, M. Ogasawara, and M. Hirose, Microelectron. Eng. 59 (2001) 373.

- [32] S. Miyazaki, M. Narasaki, M. Ogasawara, and M. Hirose, Solid-State Electronics 46 (2002) 1679.
- [33] S. Meriani (Ed.), Proceedings of the International Conference Zirconia '88. Advances in Zirconia Science and Technology. New York: Elsevier (1989).
- [34] S. Venkataraj, O. Kappertz, H. Weis, R. Drese, R. Jayavel, and M. Wuttig, J Appl Phys 92 (2002) 3599.
- [35] G. He, Q. Fang, J. X. Zhang, L. Q. Zhu, M. Liu, and L. D. Zhang, Nanotechnology 16 (2005) 1647.
- [36] L. Q. Zhu, Q. Fang, X. J. Wang, J. P. Zhang, M. Liu, G. He, and L. D. Zhang, Appl. Sur. Sci. 254 (2008) 5439.
- [37] T. Tolinski, A. Kowalczyk, G. Chelkowska, M. Mihalik, and M. Tinko, Act. Phys. Polonica A. 113 (2008) 1.
- [38] Daniel H. C. Chua, W. I. Milne, Z. W. Zhao, B. K. Tay, S. P. Lau, T. Carney, and R. G. White, J. Non-Cryst. Solids 332 (2008) 185.
- [39] John Wiley & Sons Ltd, Baffins Lane, Chichester, West Sussex PO19 1UD, England, B. Vincent Crist, Handbook of Monochromatic XPS Spectra, The Elements and Native Oxide. (2000) p515.

Korean Abstract

실리콘에 코팅된 ZrO_2 의 온도에 따른 표면현상에 관한 연구

천미선

Graduate School of Education

Pukyong National University

Abstract

실리콘 표면에 코팅된 ZrO_2 의 기판온도에 따른 표면현상에 관해 XPS, XRD, AFM, SE를 통해 연구하였다. RF sputtering의 방법으로 실리콘에 ZrO_2 를 코팅하였고 Ar과 O_2 의 비율을 1:1로 하여 기판의 온도를 상온, $100^\circ C$, $200^\circ C$, $300^\circ C$, $350^\circ C$ 로 조절하여 실험하였다. XPS를 통하여 실리콘 표면에 ZrO_2 가 코팅된 정도를 확인할 수 있었고, 기판의 온도에 따른 필름 표면의 산화상태를 알 수 있었다. 기판의 온도가 증가할수록 표면에 있는 ZrO_2 의 산화상태가 $ZrO_x(0 < x < 2)$ 에서 ZrO_2 로 변화되는 것을 관찰 할 수 있었다. XRD로는 기판의 온도에 따른 ZrO_2 의 결정구조를 확인할 수 있었다. AFM 이미지에서는 표면의 거친 정도를 알 수 있는데 기판의 온도가 증가할수록 ZrO_2 의 표면의 거친 정도가 작게 보여짐을 확인할 수 있었다. SE로는 실리콘 표면에 코팅된 ZrO_2 의 두께를 측정할 수 있었다. 온도에 따라 비교적 일정한 두께를 나타내는 것을 볼 수 있었다.

Acknowledgment

I would like to express my sincere gratitude to Prof. Yong-Cheol Kang for his continuous guidance, encouragement and advise in this study. Also, I would like to thank my referees Prof. Ju Chang Kim and Prof. Sang Yong Pyun for all their warm help and valuable comments concerning this work.

Thanks for God. I thanks to my friend Juyun Park for helping my experiment and graduate school of life. I thanks to Jin Kook Heo for helping my experiment. I thanks all graduate students, Sewon Jung, Hyun Kyung Park and Ki Soon Kim for sharing lots of precious memories for two and half years. I also thanks all my friends, Hyo Ju Moon, Hye Kyung Lim, Jee Hyun Kang, Mi Hyun Lee, Yu Jung Kang, Soo kyoung Noh, Jin Ae Choi, Hye Sun Jeong for their love and support. My thankful acknowledgements are given to church; Rev. In Sung Wang, In Young Park, Dae Up Jang, Eun Kyung Jung, Kang Yeon Lee, Yu Ree Choi for their love and pray.

My appreciations are expressed to my family members for the endless assistances.